Neighborhood-Based Recovery of Phase Unwrapping Faults

Mara Pistellato, Filippo Bergamasco, Luca Cosmo, Andrea Gasparetto, Dalila Ressi and Andrea Albarelli
Università Ca' Foscari Venezia
Dipartimento di Scienze Ambientali Informatica e Statistica
via Torino, 155 - Venice, Italy

***Abstract*—Among several structured light approaches, phase shift is the most widely adopted in real-world 3D reconstruction devices. This is mainly due to its high accuracy, strong resilience to noise and straightforward implementation. However, Phase shift also exhibits an inherent weakness, that is the spatial ambiguity resulting from the periodicity of the sinusoidal wave adopted. Of course many phase unwrapping methods have been proposed to solve such ambiguity. One of the most promising methods exploits additional signals of mutually prime periods, in order to observe a distinct combination of phases for each spatial point. Unfortunately, for such combination to be properly recognized, a very high accuracy in phase recovery must be attained for each signal. In fact, even modest errors could lead to unwrapping faults, making the overall approach much less resilient to noise than plain phase shift. With this paper we introduce a feasible and effective fault recovery method that can be directly applied to multi-period phase shift. The combined pipeline offers an optimal accuracy and coverage even with high noise conditions, overcoming the setbacks of the original method. The performance of such pipeline is established by means of an in depth set of experimental evaluations and comparison, both with real and synthetically generated data.**

I. Introduction

During the last decade, 3D sensors have gone from being a specialist tool to a product intended for the general public. In fact, the decreasing cost of components and the consolidation of fast reconstruction algorithms enabled the adoption of 3D technology in consumer products ranging from game consoles [1] to smartphones and tablets [2]. Notwithstanding the popularity of small and cheap off-the-shelf sensors, many industrial devices are still based on long-established setups. This is due to the higher accuracy level sought, which can be guaranteed only by high-end hardware, proper calibration [3], [4], [5] and top-notch signal processing. With respect to these requirements, structured light [6] is still regarded as the weapon-of-choice. Briefly, the main idea behind structured-light is the projection of a known light signal onto the objects to be captured [7]. Such signal, which is observed by one or more cameras, can then be used to assign a distinctive code to each material point in the scene. This code is the key to reconstruction, as it enables the labelling of corresponding points between different observers and thus 3D triangulation. In this paper we are not dealing with the triangulation step, which is itself a wide research topic [8], [9]. Instead, we are interested in the coding signal recovery. With respect to this problem, a deluge of different methods has been proposed

Fig. 1. Capturing of a 3D surface by means of phase shift coding.

in literature [10]. Each different approach is designed with a specific goal in mind. Some of them aim at speed, by allowing the use of a reduced number of patterns [11]. Others are focused on the ability to separate the signal from the natural texture appearing in the scene [12]. Some modern approaches went as far as using learning techniques to infer depth from the signal itself, without the need for an actual triangulation [13]. Regardless of this wide choice in coding strategies, most commercial solutions still adopt the old-fashioned phase shift method [14]. This is mainly due to its ability to provide high accuracy, resilience to noise and surface textures, great flexibility and easiness of implementation. The underlying idea is indeed quite simple: the projected frames are sine wave intensity patterns that are periodic (usually) along one direction (see Fig. 1). A total of n patterns is projected over time, each one being shifted by an offset of $\frac{2\Pi}{n}$ periods. After all the patterns have been captured by a camera, each image pixel u, v is labelled with a base phase value $\varphi(u, v) \in [0, 1)$ recovered by means of correlation (for details see for instance [15]). Unfortunately, since the signal is periodic in space, the same value of φ appears several times, one for each different sine fringe. To solve this ambiguity an additional step, commonly referred to as *phase unwrapping*, is needed. Most phase unwrapping approaches resort to the projection of an additional pattern sequence (often Gray codes), exhibiting lower accuracy, but which is not affected by ambiguity. This combined technique results in a labelling which is both unambiguous and reasonably accurate. However, such methods have the drawback that not all the projected patterns effectively contribute to the accuracy of φ. To allow a better exploitation of captured signals, some authors proposed multi-period approaches which use phase shift also for disambiguation (for instance [16]). While promising, these latter techniques are seldom adopted in actual devices. In fact, as we will show in the experimental section, they are quite sensitive to noise as the unwrapping step requires an extremely high accuracy in phase recovery.

With this paper we introduce a practical method to address such noise sensitivity. The resulting pipeline enables the practical adoption of multi-period phase shift with a minimal effort and guarantees maximal accuracy at any noise level.

II. Multi-period Phase Shift

Multi-period phase shift, proposed by Lilienblum and Michaelis [16], combines phase recovery and unwrapping by mean of n independent phase shift sequences of different (and possibly coprime) period lengths $\lambda_1, \lambda_2, ..., \lambda_n$, resulting in a vector of recovered phases $\boldsymbol{\varphi} = (\varphi_1\ \varphi_2\ ...\ \varphi_n)^T$. The main idea, depicted in Fig. 2, is that, given an unique projector coordinate ξ, the phases vector $\boldsymbol{\varphi}$ will be also unique. In fact, the same combination of phases will not appear again until $\xi'' = \xi' + k\ \xi_{max}$, where $\xi_{max} = LCM(\lambda_1, \lambda_2, ..., \lambda_n)$ (that is the Least Common Multiple of all period lengths).

More in detail, we can define functions $\varphi_i(\xi)$ and $\eta_i(\xi)$ respectively as phase value and fringe number expected to be recovered from projector coordinate ξ by the i^{th} pattern sequence:

$$\eta_i(\xi) = \left\lfloor \frac{\xi}{\lambda_i} \right\rfloor \qquad \varphi_i(\xi) = \frac{\xi}{\lambda_i} - \left\lfloor \frac{\xi}{\lambda_i} \right\rfloor \tag{1}$$

From these definitions we can infer the following system of equations

$$\xi = (\eta_i(\xi) + \varphi_i(\xi))\lambda_i \qquad \forall i = 1, ..., n \tag{2}$$

After the patterns have been projected and the phases $\varphi_i(\xi)$ recovered, the only unknowns left are the components of the fringe numbers $\boldsymbol{\eta} = (\eta_1(\xi)\ \eta_2(\xi)\ ...\ \eta_n(\xi))^T$ and the projector coordinate ξ itself. Imposing the condition $\xi < \xi_{max}$, the system has an unique solution, thus allowing to recover the sought projector coordinate ξ.

Such unique solution can be easily found by considering the differences between phases. Specifically, fixing two pattern sequences j and k, the right sides of the equations in system (2) can be equated, obtaining:

$$\begin{aligned} (\eta_j(\xi) + \varphi_j(\xi))\lambda_j &= (\eta_k(\xi) + \varphi_k(\xi))\lambda_k \\ \lambda_j\eta_j(\xi) - \lambda_k\eta_k(\xi) &= \lambda_k\varphi_k(\xi) - \lambda_j\varphi_j(\xi) \end{aligned} \tag{3}$$

In particular, from the right part of such relation, we can define a phase difference vector based on the offset from pattern sequence 1:

$$\Phi(\xi) = \boldsymbol{a} = (a_1, ..., a_n); \qquad a_i = \lambda_1\varphi_1(\xi) - \lambda_i\varphi_i(\xi) \tag{4}$$

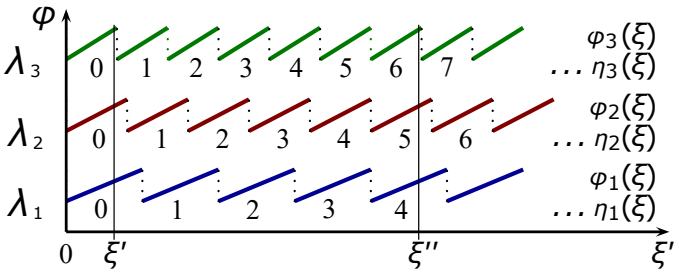

Fig. 2. Disambiguation principle in multi-period phase shift.

Since we already limited the code values, elements a_i are not ambiguous and a map H can be defined in the following way:

$$H(\boldsymbol{a}) = \begin{cases} (h_1, h_2, ..., h_n): & \forall i\{a_i = \lambda_i h_i - \lambda_1 h_1\} \\ \text{undefined} & \text{otherwise} \end{cases} \tag{5}$$

allowing for an easy conversion between phase difference vectors and fringe numbers:

$$H(\Phi(\xi)) = (\eta_1(\xi), \eta_2(\xi), ..., \eta_n(\xi)) \tag{6}$$

The range of values in H is a finite set, which depends only on period lengths $\lambda_1, ..., \lambda_n$. Therefore, it is possible to pre compute all the values for H and store them in a LUT (Look Up Table). This data structure allows to compute fringe numbers in a fast way given the sequence of phase observations $\boldsymbol{\varphi}$.

Of course, in the real-world $\boldsymbol{\varphi}$ will be affected by errors due to several error sources. So it is not obvious that $\Phi(\xi)$ will be accurate enough for H to map it to the correct fringe vector. As a matter of fact, as we show in Sec. IV, even modest levels of noise lead to difference vectors that are not in the domain of eq. 5. This, in turn, leads to LUT access faults and, in general, to the inability of recovering the correct value for ξ (see [16] for details). It should be noted that, once the LUT access fails, the difference vector offers no hint about where to search for a fringe vector that would justify the obtained $\boldsymbol{\varphi}$. To this end, a brute force solution would be to check for all the feasible combinations of fringe values and select the one that minimizes the radius of estimated ξ. Unfortunately this would lead to a huge number of tests. In the following section we propose three strategies to reduce the number of fringe vectors to be checked.

III. Neighborhood-based Fault Recovery

The following strategies are actually rather naive. However, the main contribution of this paper is about their evaluation in terms of effectiveness and feasibility with respect to computational efficiency. Our goal, indeed, is to show that multi-period phase shift can be easily adopted in real-world scenarios without drawbacks.

The shared mechanics of all the following strategies involves the selection of a reduced set of fringe vectors $\boldsymbol{\eta}$ to be tested, that we call S_η, and a rule to extract among its elements the optimal fringe vector $\boldsymbol{\eta}^*(S_\eta)$.

For a given vector of observed phases $\boldsymbol{\varphi}$ and a fringe vector $\boldsymbol{\eta} \in S_\eta$, we define an estimation for both the projector coordinate ξ and its error ϵ. The obvious estimator for ξ is the average of the independent values obtained from each period sequence. According to eq. 2, it can be computed as:

$$\xi(\boldsymbol{\varphi}, \boldsymbol{\eta}) = \frac{\sum_{i=1}^{n}(\eta_i(\xi) + \varphi_i(\xi))\lambda_i}{n} \tag{7}$$

One of the main advantages of eq. 7 is that, assuming that no outliers are present, each single pattern equally contributes to a better assessment of ξ.

A reasonable estimator for the error of $\xi(\boldsymbol{\varphi}, \boldsymbol{\eta})$ could be of course the standard deviation exhibited by the averaged values.

However, since the number of signals involved in multi-period phase shift is usually small, we opted for a more conservative choice. We assess the error commited as the radius of the independent estimates for ξ, that is:

$$\epsilon(\boldsymbol{\varphi}, \boldsymbol{\eta}) = \max_{1 \leq i,j \leq n} |(\eta_i(\xi) + \varphi_i(\xi))\lambda_i - (\eta_j(\xi) + \varphi_j(\xi))\lambda_j| \quad (8)$$

The optimal fringe vector can thus be found as:

$$\boldsymbol{\eta}^*(S_\eta) = \arg \min_{\boldsymbol{\eta} \in S_\eta} \epsilon(\boldsymbol{\varphi}, \boldsymbol{\eta}) \quad (9)$$

Consequently, the optimal estimate for ξ within the set of candidates S_η is $\xi(\boldsymbol{\varphi}, \boldsymbol{\eta}^*(S_\eta))$. Additionally, we also define a general criterion to be adopted in order to retain or discard such estimates. This is needed because if no valid candidate for $\boldsymbol{\eta}$ exists in S_η, then the obtained value for ξ could be totally random. Since this is just an outlier detection measure, the criterion can be very coarse. In this paper we adopt a threshold t_ϵ over $\epsilon(\boldsymbol{\varphi}, \boldsymbol{\eta})$. To this end $\xi(\boldsymbol{\varphi}, \boldsymbol{\eta}^*(S_\eta))$ is considered recovered only if $\epsilon(\boldsymbol{\varphi}, \boldsymbol{\eta}^*(S_\eta)) < t_\epsilon$. Otherwise, the point is deemed to be non-recoverable. We propose to set $t_\epsilon = 0.5\,(\sum_{i=1}^{n} \lambda_i)/n$. This is a quite coarse estimate, since the typical error is much lower than half the average period length. Still in all our experiments this threshold never resulted in an outlier accepted as a valid ξ.

A. Vector Fringe Consesus

All the strategies proposed to build S_η for a pixel (u, v) works by looking at the neighborhood of the pixel itself. We define $N_k(u, v)$ as the set of the k nearest pixels to (u,v) that are correctly mapped using map H. Moreover, we define $N_k(u, v, \boldsymbol{\eta})$ as the set of pixels in $N_k(u, v)$ that are mapped by H to $\boldsymbol{\eta}$ and we say that $\boldsymbol{\eta} \in N_k(u, v)$ if $|N_k(u, v, \boldsymbol{\eta})| > 0$.

The Vector Fringe Consensus strategy (VFC) defines the set of fringe vectors to be checked as:

$$S_{vfc}(u, v) = \{\boldsymbol{\eta} \,|\, |N_k(u, v, \boldsymbol{\eta})| \geq |N_k(u, v, \boldsymbol{\eta'})|\,, \forall \boldsymbol{\eta'}\} \quad (10)$$

This means that all the most frequent vectors in the neighborhood of (u, v) are checked.

B. Independent Fringe Consesus

We define $N_k(u, v, \eta, i)$ as the set of pixels in $N_k(u, v, \boldsymbol{\eta})$ such that $\eta_i = \eta$ for any $\boldsymbol{\eta}$, and the set of best candidates for a given fringe i as:

$$S^i_{ifc}(u, v) = \{\eta \,|\, |N_k(u, v, \eta, i)| \geq |N_k(u, v, \eta', i)|\,, \forall \eta'\} \quad (11)$$

This means that each set $S^i_\eta(u, v)$ contains the most frequent fringe numbers for period i within the set $N_k(u, v)$.

Using these sets, the Independent Fringe Consensus strategy (IFC) defines the set of fringe vectors to be checked as:

$$S_{ifc}(u, v) = \prod_{i=1}^{n} S^i_{ifc}(u, v) \quad (12)$$

That is the Cartesian product of all the sets $S^i_{ifc}(u, v)$.

It should be noted that the set $S_{ifc}(u, v)$ is not necessarily a super set of $S_{vfc}(u, v)$ as there is no guarantee that the most frequent combinations as whole fringe vectors $\boldsymbol{\eta}$ are composed of the most frequent independent components. Indeed, the rationale of IFC is to decouple single coordinate of $\boldsymbol{\eta}$ in order to deal with corner cases including fringe boundaries, where only one or two fringe numbers actually changes.

C. Complete Fringe-set Check

The third strategy is the most exhaustive, since it checks all the possible combinations of fringe numbers that appear in the neighborhood of the pixel. To this end, we first define the set of single fringe coordinates as:

$$S^i_{cfc}(u, v) = \{\eta \,|\, |N_k(u, v, \eta, i)| > 0\} \quad (13)$$

In a similar manner to IFC, also the complete Fringe-set Check strategy (CFC) defines a set of fringe vectors to be checked as a Cartesian product:

$$S_{cfc}(u, v) = \prod_{i=1}^{n} S^i_{cfc}(u, v) \quad (14)$$

This time, however, for a fringe number to be included it has just to be present in at least one neighbor. This is a very relaxed constraint and it is not clear if such allowance would result in an unfeasible number of fringe vectors to check. As we will show in the experimental section, this is not the case and the number of actual fringe combination to validate is in practice quite modest.

IV. Experimental evaluation

The proposed approach is introduced in order to solve a practical problem with multi-period phase shift. To this end, it is paramount to assess its effectiveness with an in depth experimental evaluation.

In this section we perform such analysis with a set of different goals in mind. First of all, we want to show the ability of our method in recovering unwrapping faults both in terms of percentage of recovered points and of their accuracy. Then, we demonstrate that such ability is not critically affected by the number of candidates inspected, and thus the method can be applied without a significant performance loss. Finally a proper comparison with a standard non multi-period approach is reported. This last test highlights the improvement in accuracy granted by the redundant information offered by different (and independent) signals.

A. Fault Recovery with Noisy Signal

For an useful evaluation of the effectiveness of our method as a recovery tool, it is very important to know exactly the expected fringe numbers η_i for each given image pixel. This is hard to obtain accurately with real-world scans since it would require to perfectly know the geometry of the observed object, of the projector frustum and the relative pose of camera and projector. On the other hand, real-world observation is not critical to the relevance of this evaluation. In fact, the error committed with the reconstruction of each phase φ_i is indeed the only factor affecting the unwrapping step of multi-period phase shift. Such error can originate by various sources, however, at the end of the day, the only significant element is

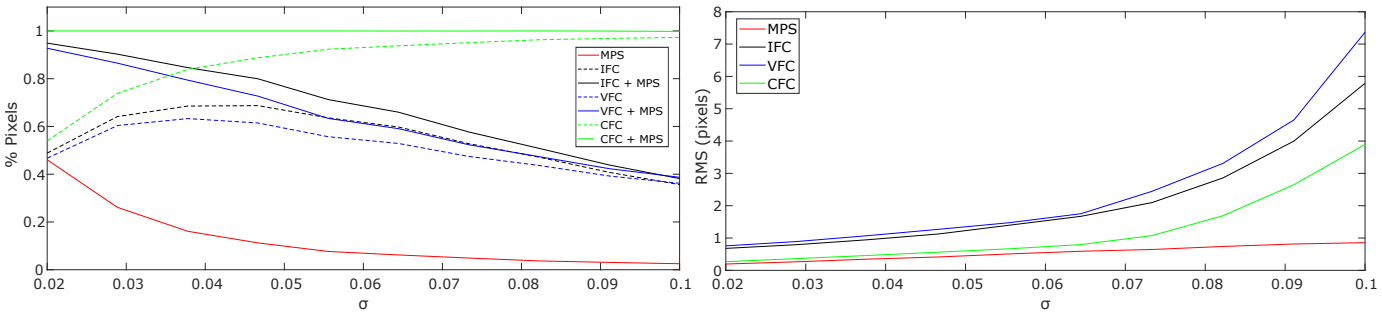

Fig. 3. Comparison of the recovery rate and resulting RMS error achieved by the proposed methods.

its magnitude. If we model the error as zero-mean Gaussian additive noise, such magnitude can be expressed as a standard deviation σ and we can evaluate the resilience to noise by simulating perturbed phase observations:

$$\tilde{\varphi}_i = \frac{\xi}{\lambda_i} - \left\lfloor \frac{\xi}{\lambda_i} \right\rfloor + N(0,\sigma) \qquad i \in 1..n \tag{15}$$

where ξ is a randomly generated projector coordinate, n is the total number of periods and $N(0,\sigma)$ is a normally distributed unbiased random variable with standard deviation σ. We also assume the noise magnitude σ to be identical for all the phase observations, which is reasonable since it mainly depends on the number of samples, which is usually the same for all the periods.

In our first batch of experiments we generated 10^6 samples for different values of σ and an amount of neighbors checks fixed to 10. We applied respectively IFC, VFC and CFC to recover the faults from plain multi-period phase shift (MPS). We classified a point as recovered when a method assigns to it the correct set of fringe numbers. The results are shown on the left plot of Fig. 3. The red line represents the amount of points correctly unwrapped by MPS at the first round. The dotted lines show the amount of points respectively recovered by IFC, VFC and CFC and the continuous lines of the same color the total number of unwrapped points by combining the initial set with the ones recovered by each method. There are several observation that can be made by looking at this data. First of all, even with a small amount of noise (about 2% over the normalized phase value), MPS fails about 50% of the times. This is a well-known limitation of MPS, which indeed reduces greatly its feasibility in real-world products. Interesting enough, both IFC and VFC work reasonably with low noise levels, still their performance drops fast. The failure of VFC means that with high noise levels it is difficult for the correct fringe vector to consinstenly gain major consensus. In a similar manner, the failure of IVC means that even by seeking independently the consensus for each phase component, it is quite common to obtain a broken vector. This effect is likely due to the fact that each phase is independently observed and thus the probability of getting a full set of n correct consensus over fringes, gets smaller as n increases.

Differently, CFC works remarkably well also with a very high noise level. As a matter of fact it is able to recover all the correct fringes even when MPS offers less than 10% of unwrapped points. This is partially expected, since for CFC to work it is required that the correct fringe appers at least in one neighbor. This is a very loose requirement, given that the observations are independent and the probability of not getting the correct fringe in n neighbors decreases quickly with n.

While this is a very encouraging result, the recovery of the unwrapping does not automatically implies a good accuracy. Undoubtedly the overall error obtained by combining errors in phase recovery when computing the average ξ could still lead to an unacceptable result. To analyze the overall accuracy we plotted, in the right part of Fig. 3, the RMS error of the recovered points with respect to the ground-truth.

By looking at the plot it seems that CFC offers consistently better accuracy than IFC and VFC. Specifically, the accuracy of CFC is actually comparable with the degree of precision obtained by points directly unwrapped by MPS at the first round. The breaking point seems to be around a standard deviation on the synthetically-generated data of about 6%, which is indeed huge (about $\frac{1}{3}$ radians). Note also that, until that point, the recovery error is around a half code unit, which in practice corresponds to sub-pixel accuracy in projector coordinates. Finally, it should also be noted that the slow increase in the error exhibited by MPS after the 6% threshold is not really due to some particular merit, but its a simple consequence of the implied biased selection. In fact, only the observation characterized by low error are actually unwrapped by MPS at the first round.

B. *Effect of the Number of Neighbor Checks*

At this point CFC appears to be the best candidate for unwrapping faults recovery. However, since it works on the complete Cartesian product of fringe observation sets, it could end up checking much more candidates than IFC and VFC. For

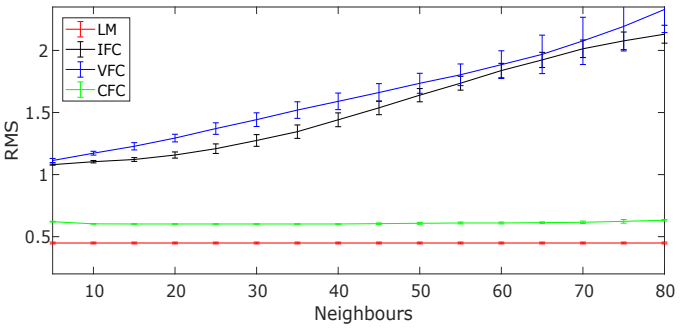

Fig. 4. Analysis of the accuracy obtained with different values of parameter k (i.e. amount of tested neighbors).

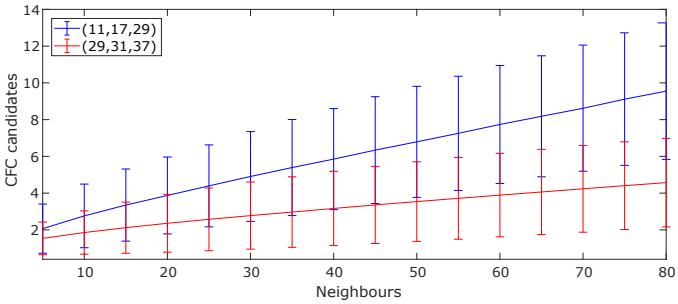

Fig. 6. Number of candidate vectors actually tested by CFC for different values of parameter k.

this reason, it is very important to verify that its accuracy can be achieved without needing an extensive search. To this end, we performed a batch of tests by setting the noise level at 6% and by exploring the effect of different choices for parameter k, that is the number of decoded surrounding pixels to be considered. The results are shown in Fig. 4. It can be noted that the number of neighbors has actually a very limited effect on CFC, which is of course an important feature. In detail, while a choice of only 5 neighbors implies a slight drop in performance, 10 check points seem to be more than enough. Finally, we can observe an interesting phenomenon appearing when the number of checked neighbors grows too much. As a matter of fact, a large amount of neighbors results indeed in a slightly diminished accuracy and a larger standard deviation. This is probably due to the fact that, when the product set becomes very large, it could happen randomly that a wrong fringe number configuration is blessed by a higher coherency than the correct one. This is an important observation, in fact it offers an additional reason (beside computational feasibility) to avoid the naive approach of checking all the possible fringe configurations.

Regarding the computational feasibility of CFC, we are also interested in assessing how many candidates result from different number of neighbors checks. This is shown in Fig. 6 for two different sets of period lengths. The number of actual candidates exhibits a large variance, since it depends a lot on the position of the observed point. Still, its magnitude is in general quite low and grows in a linear manner with the size of the neighbor set. In practice, since 10 neighbors have been shown to be a reasonable choice for a good performance of CFC, we can conclude that the recovery step would require to check a very small amount of candidates, with minimal impact in the overall execution time of the full pipeline over plain MPS.

C. Real-World Evaluation

In the previous sections we adopted synthetically generated data to enable an evaluation under controlled conditions of noise and with a well defined ground-truth. Nevertheless, for a complete validation of the approach a demonstration of its effectiveness with an actual camera-projector setup is needed. To this end, we used a calibrated camera-projector pair composed of a CCD machine vision camera with 3Mpixels resolution, a full hd video projector and a disparity of about 20cm. The system was calibrated using [17] and verified using artificial markers [18], [19]. Since a proper ground-truth could not be available, we evaluated the performance by capturing planar surfaces of different materials and then by computing the average distance of each reconstructed point from an ideal plane obtained by fitting all the points reconstructed by using only MPS. This should be a reasonable substitute for a ground-truth since its a statistical measure based on a large number of reliable points. Since it's not possible to set the amount of desired noise in such kind of experiment, we evaluated the RMS error with respect to the plane for different amounts of samples used for phase recovery. Under these conditions, the phase recovery error, and thus the observation noise, is expected to decrease with the square root of the number of samples. The results are shown in Fig. 5, by mean of two plots similar to those shown in Fig. 3. The observed trends confirm those obtained with synthetically generated data. Finally, in Fig. 7 we also show actual reconstruction examples to supply a basic intuition about the real effects of the different recovery rates and accuracy levels. The items reconstructed are a set of planar surfaces placed at a distance of about 1 meter from the projector-camera system.

D. Comparison with gray coding

As discussed, multi-period phase shift is very sensitive to noise. In fact, even a naive approach using a single phase shift, combined with gray coding disambiguation, can lead to more stable unwrapping results. Moreover, approaches designed to deal with the few unwrapping errors from gray coding have

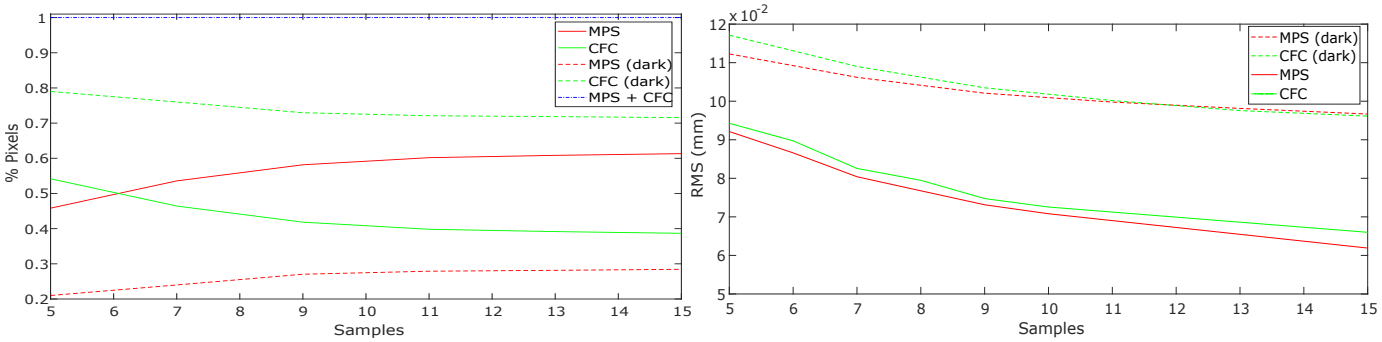

Fig. 5. Comparison of the recovery rate and resulting RMS error achieved by CFC and MPS with a real plane.

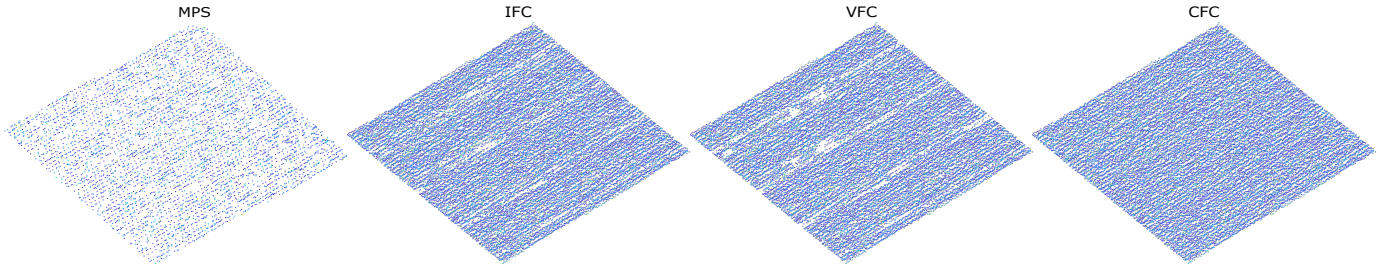

Fig. 7. Examples of reconstruction of difficult surfaces using plain MPS (1st column), IFC (2nd column), VFC (3rd column) and CFC (4th column).

already been proposed in literature [20]. For this reason the practitioner could ask if there is any compelling reason to adopt our CFC extension of MPS. Actually there is a really important difference between the two approaches. When gray coding is used for disambiguation, the projected patterns do not contribute to the accuracy of the coding. In fact they are simply discarded once the fringe number for a point is recovered. Differently, with multi-period phase shift, and thus with CFC, all the single observed phases provide useful information. In Fig. 8 we report the result of an experiment performed with the same setup presented in Sec. IV-A, comparing the RMS error with respect to ground-truth obtained with CFC and the technique presented in [20]. The standard deviation of the noise is set to 6%. We applied this error to all the phases recovered with CFC (over three periods) and to the single phase observed by the state-of-the-art method [21]. In addition we assumed the unwrapping from gray coding to be always perfect. The advantage of CFC in terms of accuracy is quite prominent.

V. Conclusion

With this paper we examined three strategies for phase unwrapping faults recovery. Among these, Complete Fringe-set Check (CFC) exhibited the best behavior and we think it to be suitable to be adopted in practical scenarios. In fact, despite being rather simple, it definitely fixes a long standing problem with multi-period phase shift methods: the inherent high sensitivity to noise. The effectiveness, efficiency and accuracy of CFC has been demonstrated by means of a thorough experimental evaluation performed over both real and synthetically generated data.

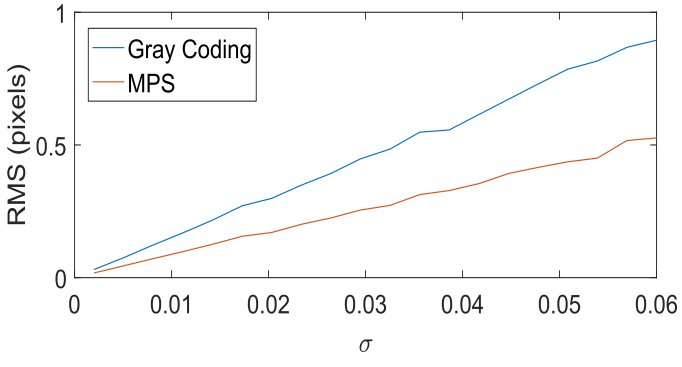

Fig. 8. Enhanced accuracy of MPS/CFC with respect to gray coding

References

[1] J. Han, L. Shao, D. Xu, and J. Shotton, "Enhanced computer vision with microsoft kinect sensor: A review," *IEEE Transactions on Cybernetics*, vol. 43, no. 5, pp. 1318–1334, 2013.

[2] W. Winterhalter, F. Fleckenstein, B. Steder, L. Spinello, and W. Burgard, "Accurate indoor localization for rgb-d smartphones and tablets given 2d floor plans," vol. 2015-December, 2015, pp. 3138–3143.

[3] F. Bergamasco, L. Cosmo, A. Albarelli, and A. Torsello, "Camera calibration from coplanar circles," in *ICPR 2014*, 2014, pp. 2137–2142.

[4] F. Bergamasco, A. Albarelli, L. Cosmo, A. Torsello, E. Rodolà, and D. Cremers, "Adopting an unconstrained ray model in light-field cameras for 3d shape reconstruction," in *CVPR 2015*, 2015, pp. 3003–3012.

[5] M. Pistellato, A. Albarelli, F. Bergamasco, and A. Torsello, "Robust joint selection of camera orientations and feature projections over multiple views," in *ICPR 2016*, 2017, pp. 3703–3708.

[6] R. Valkenburg and A. McIvor, "Accurate 3d measurement using a structured light system," *Image and Vision Computing*, vol. 16, no. 2, pp. 99–110, 1998.

[7] F. Chen, G. Brown, and M. Song, "Overview of three-dimensional shape measurement using optical methods," *Optical Engineering*, vol. 39, no. 1, pp. 10–22, 2000.

[8] R. Hartley and A. Zisserman, *Multiple view geometry in computer vision*. Cambridge university press, 2003.

[9] F. Bergamasco, L. Cosmo, A. Albarelli, and A. Torsello, "A robust multi-camera 3d ellipse fitting for contactless measurements," in *3DIMPVT 2012*, 2012, pp. 168–175.

[10] J. Salvi, J. Pagès, and J. Batlle, "Pattern codification strategies in structured light systems," *Pattern Recognition*, vol. 37, no. 4, pp. 827–849, 2004.

[11] S. V. der Jeught and J. J. Dirckx, "Real-time structured light profilometry: a review," *Optics and Lasers in Engineering*, vol. 87, no. Supplement C, pp. 18 – 31, 2016.

[12] M. Vo, S. G. Narasimhan, and Y. Sheikh, "Texture illumination separation for single-shot structured light reconstruction," *IEEE Trans. Pattern Anal. Mach. Intell.*, vol. 38, no. 2, pp. 390–404, Feb. 2016.

[13] S. R. Fanello, C. Rhemann, V. Tankovich, A. Kowdle, S. O. Escolano, D. Kim, and S. Izadi, "Hyperdepth: Learning depth from structured light without matching," pp. 5441–5450, June 2016.

[14] V. Srinivasan, H. C. Liu, and M. Halioua, "Automated phase-measuring profilometry of 3-d diffuse objects," *Appl. Opt.*, vol. 23, no. 18, pp. 3105–3108, Sep 1984.

[15] Y. Surrel, "Design of algorithms for phase measurements by the use of phase stepping," *Applied optics*, vol. 35, no. 1, pp. 51–60, 1996.

[16] E. Lilienblum and B. Michaelis, "Optical 3d surface reconstruction by a multi-period phase shift method," *JCP*, vol. 2, no. 2, pp. 73–83, 2007.

[17] D. Moreno and G. Taubin, "Simple, accurate, and robust projector-camera calibration," in *3DIMPVT 2012*, 2012, pp. 464–471.

[18] F. Bergamasco, A. Albarelli, L. Cosmo, E. Rodola, and A. Torsello, "An accurate and robust artificial marker based on cyclic codes," *PAMI*, vol. 38, no. 12, pp. 2359–2373, 2016.

[19] F. Bergamasco, A. Albarelli, and A. Torsello, "Image-space marker detection and recognition using projective invariants," in *3DIMPVT 2011*, 2011, pp. 381–388.

[20] D. Zheng and F. Da, "Self-correction phase unwrapping method based on gray-code light," *Optics and Lasers in Engineering*, vol. 50, no. 8, pp. 1130 – 1139, 2012.

[21] D. Zheng, F. Da, Q. Kemao, and H. S. Seah, "Phase-shifting profilometry combined with gray-code patterns projection: unwrapping error removal by an adaptive median filter," *Opt. Express*, vol. 25, no. 5, pp. 4700–4713, Mar 2017.